Appl. Phys. A (2015) 118:353–359
DOI 10.1007/s00339-014-8740-5

Applied Physics A
Materials Science & Processing

Temperature-dependent electrical properties for graphene Schottky contact on n-type Si with and without sulfide treatment

Yow-Jon Lin · Jian-Jhou Zeng · Hsing-Cheng Chang

Received: 12 July 2014 / Accepted: 13 August 2014 / Published online: 28 August 2014

Abstract The temperature-dependent current–voltage (*I–V*) characteristics of graphene/n-type Si Schottky diodes with and without sulfide treatment were measured in the temperature range of 150–420 K. The temperature dependence of forward-bias *I–V* characteristics can be explained on the basis of the thermionic emission theory by assuming the presence of Gaussian distribution of the barrier heights. The graphene/n-type Si device with sulfide treatment exhibits a good rectifying behavior with the ideality factor of 1.8 and low leakage at 300 K. The enhanced device performance is considered to mainly come from the presence of Si–S bonds that serve to improve the Schottky barrier inhomogeneity. Compared to the fitting data for the temperature-dependent reverse-bias *I–V* characteristics of graphene/n-type Si devices without sulfide treatment, the fitting data for the temperature-dependent reverse-bias *I–V* characteristics of graphene/n-type Si devices with sulfide treatment show that a higher barrier height for hopping result in a lower leakage current. This is because of more homogenous barrier height for graphene/n-type Si devices with sulfide treatment.

1 Introduction

Graphene, which is a zero-gap semiconductor having a high intrinsic carrier mobility, is considered one of the most promising candidates for future semiconductor industry applications because of its extraordinary properties. Based on its unique electrical properties, a number of works on electronic device applications have been carried out [1–9]. Due to the technological importance of Schottky diodes which are among the most simple of the graphene–Si contact devices, a full understanding of the nature of their electrical characteristics is of great interest. It has been suggested that charge puddles may be responsible for the presence of inhomogeneous Schottky barrier height in the graphene/Si devices, which property still remains not fully understood [9]. For this study, the current–voltage (*I–V*) curves of graphene Schottky contact on n-type Si (n-Si) with and without sulfide treatment are measured and compared at various temperatures, in order to understand the carrier conduction mechanisms. In recent years, solar cells, Schottky diodes and memory devices based on the n-Si samples have attracted great interest [3, 6–8, 10–19]. Si has been a popular material of choice because it is very abundant, non-toxic, and has a rich history in advanced electronics. The investigation of the temperature-dependent *I–V* characteristics of graphene/n-Si Schottky diodes to find the inhomogeneous barrier height was developed in this study. Correlation effects were evaluated using the well-known expressions for thermionic emission (TE) [8, 12, 15, 20] and the hopping conduction. By analyzing these experimental results, we shall discuss on the possible sources of Schottky barrier inhomogeneity.

2 Experimental procedure

Four-inch n-Si (100) wafers with resistivity in the range of 1–10 Ω cm purchased from Woodruff Tech Company were used in the experiment. The n-Si film thickness was about

Y.-J. Lin (✉) · J.-J. Zeng
Institute of Photonics, National Changhua University of Education, Changhua 500, Taiwan
e-mail: rzr2390@yahoo.com.tw

H.-C. Chang
Department of Automatic Control Engineering, Feng Chia University, Taichung 407, Taiwan

525 μm. The n-Si samples were cleaned in chemical cleaning solutions of acetone and methanol, rinsed with de-ionized water, and blow-dried with N_2. Next, the n-Si sample was chemically etched with a diluted HF solution for 1 min, rinsed with de-ionized water and blow-dried with N_2 (referred to as as-cleaned n-Si samples). Then, some of the as-cleaned n-Si samples were dipped into a yellow $(NH_4)_2S_x$ solution (with 6 % S, Nippon Shiyaku Co., Ltd.) for 5 min (referred to as sulfide-treated n-Si samples). Before the CVD growth of graphene, the copper foil (90 μm thick) was preannealed at 1,000 °C for 30 min under a flow of $H_2 = 9$ SCCM (SCCM denoted standard cubic centimeter per minute) in order to prepare a high-density terrace structure on Cu. A gas mixture of CH_4 (120 SCCM) and H_2 (40 SCCM) was used for the growth of graphene at 66.7 Pa [8, 21]. After 40 min of growth, the system was cooled to room temperature under H_2. To transfer the as-grown graphene sheets, a polymethylmethacrylate (PMMA) layer was spin coated on the graphene/Cu sample. The PMMA/graphene/Cu sample was then baked at 100 °C for 1 min. The procedures from coating to drying were repeated five times. Next, the sample was immersed in the $FeCl_3$ solution (0.1 g/cm^3) for 6 h overnight to remove the Cu substrates. The PMMA/graphene layers were, respectively, transferred to n-Si substrates with and without sulfide treatment, and the PMMA layer was finally dissolved by acetone. The graphene/n-Si samples were then inserted into a furnace and annealed in pure nitrogen ambience at 200 °C for 1 min. The graphene area is 0.5 × 0.5 cm^2. In ohmic contacts were deposited onto the back surface of n-Si by a sputter coater. The *I–V* curves were measured using a Keithley Model-4200-SCS semiconductor characterization system. The *I–V* characteristics of the devices were measured in the temperature range of 100–500 K using a temperature controlled cryostat, which enables us to make measurements in the temperature range from 150 to 420 K by steps of 30 K. The structural property of graphene was examined using Raman spectroscopy (Ramboss 500i, DongWoo Optron). A 532-nm laser was used for excitation.

3 Results and discussion

Figure 1 shows the Raman spectra of the graphene/Cu and graphene/n-Si samples, respectively. Although the Raman spectra do not present a flat background for graphene/Cu samples, the Raman features are still clear. The background is assigned to the surface plasmon emission of copper, with a maximum around 600 nm [22], which corresponds to the photoluminescence of copper [23]. However, the presence of the broad photoluminescence band in the Raman spectra shown in Fig. 1 can be easily overcome by performing a background subtraction during the data analysis process [23]. Graphene displays a band at ~1,345 cm^{-1}, a band at ~1,580 cm^{-1} and a band at ~2,700 cm^{-1} corresponding to the well-documented D, G and 2D bands [4, 7, 24–26]. The G band is assigned to the E_{2g} mode of the relative motion of sp^2 carbon atoms. The intensity of the 2D band is related to the layer numbers of graphene [24–26]. The ratio of the 2D–G peak intensities was calculated to be close to 1, suggesting that four layers of graphene formed [24–26]. The D band caused by the disorder band in graphite edge is seen in the Raman spectra [27], which indicates the structural imperfection induced by hydroxyl and epoxide groups on the carbon basal plane [28] and electron trapping adsorbate groups (possibly O_2^- or H_2O^- derived) on the graphene surface [29] that serve to increase the work function [21]. Lin and Zeng [21] found that the work-function value of defective graphene (4.9 eV) is larger than the reported value (4.6 eV) [4] of undoped graphene. We deduce that defective graphene transferred onto the n-Si substrate may lead to the increased Schottky barrier height at the graphene/n-Si interfaces. In addition, the amount of disorder in graphene is often correlated with the intensity of the D band [4]. The ratio of the D–G peak intensities (I_D/I_G) is usually used to evaluate the disorder of graphene. For graphene/Cu and graphene/n-Si samples, the I_D/I_G ratio is about 0.42, implying that techniques to transfer graphene onto the n-Si substrate did not induce disorder in graphene.

Figure 2 shows the temperature-dependent *I–V* characteristics of the graphene/as-cleaned n-Si and graphene/sulfide-treated n-Si Schottky diodes, respectively. The rectifying *I–V* characteristics suggest that Schottky junctions are formed at the graphene/n-Si interfaces. The

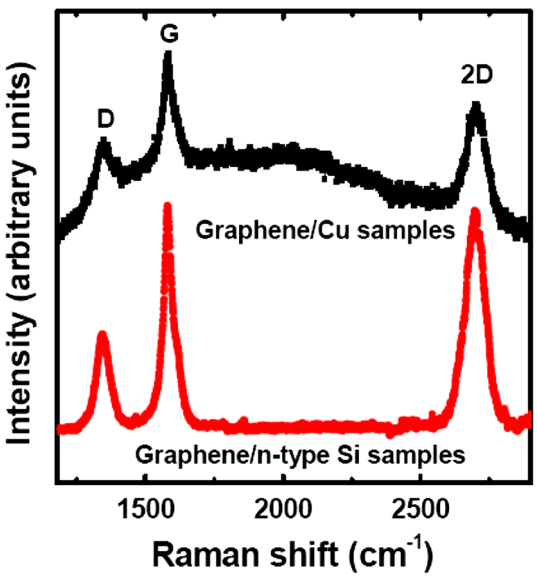

Fig. 1 Raman spectra of graphene/Cu and graphene/n-Si samples

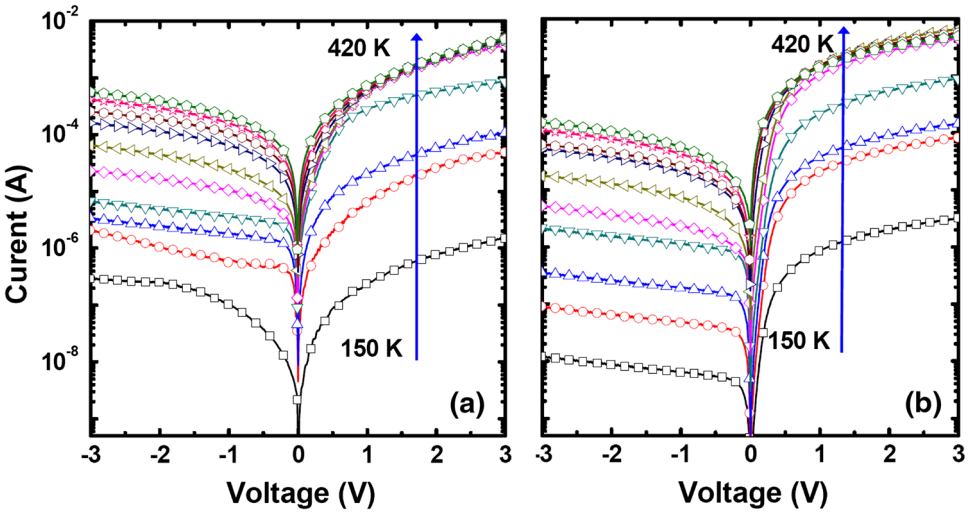

Fig. 2 Temperature-dependent *I–V* curves of **a** graphene/as-cleaned n-Si and **b** graphene/sulfide-treated n-Si Schottky diodes

processing steps used to transfer the CVD-grown graphene typically result in p-doped material with the higher work function than 4.6 eV [8, 21]. The larger work function of graphene (>4.6 eV) than the electron affinity of Si (4.05 eV) may lead to the formation of a Schottky junction at the graphene/n-Si interface. From the TE theory, the *I–V* characteristic of a Schottky diode is given by [8, 12, 15, 20]

$$I = I_s\left[\exp\left(\frac{qV}{\eta kT}\right) - 1\right] = SA^*T^2\exp\left(-\frac{q\phi_B}{kT}\right)\left[\exp\left(\frac{qV}{\eta kT}\right) - 1\right], \quad (1)$$

where S is the Schottky contact area, η is the ideality factor, q is the electron charge, $q\phi_B$ is the Schottky barrier height, T is the absolute temperature, k is the Boltzmann constant and A^* is the effective Richardson constant (114 A cm^{-2} K^{-2} for n-Si) [20]. η is determined from the slope of the linear region of the forward-bias ln(I)–V characteristics. The values of η and $q\phi_B$ were derived from the curve fitting of *I–V* characteristic.

Figure 3a shows η ($q\phi_B$) as a function of temperature. In agreement with the previously reported results for graphene/n-Si Schottky diodes [3, 6–8, 19], we found that the extracted room-temperature $q\phi_B$ values were varied in the range of 0.6–0.8 eV. For graphene/n-Si Schottky diodes without sulfide treatment, $\eta > 2$ is found at different temperatures, suggesting that defects at the interface may play important roles in the conduction process. However, sulfide treatment may lead to a remarkable reduction in η and an increase in $q\phi_B$. It is shown that $q\phi_B$ decreases and η increases with the decrease temperatures. According to the Tung's model [30], both η of more than 1 and its linearity vs. 1,000/T can be convincing evidence of an inhomogeneous barrier height. In addition, the variation in η with temperature is called the T_o effect [31]. Figure 3b shows η as a function of 1,000/T and the linear fitting curve. Such behaviors of the diode ideality factor have been attributed to particular distribution of states at the n-Si surface [32]. η of the diodes showing this behavior varies with temperature as; $\eta = \eta_o + (T_o/T)$ [31]. The η_o and T_o of graphene/n-Si (graphene/sulfide-treated n-Si) Schottky diodes are constants which were found to be 1.97 (1.23) and 704.5 (172.9) K, respectively. Sulfide treatment led to reductions in η_o and T_o. The smaller values of η_o and T_o correspond to more homogenous barrier height. The spatially inhomogeneous barriers and potential fluctuations at the interface consist of low and high barrier areas, that is, the current through the diode will flow preferentially through the lower barriers in the potential distribution [32]. The inhomogeneous barriers and potential fluctuations may be related to interface states. An explanation to the origin of graphene–Si interface state is provided by the dangling bonds at the n-Si surfaces. Figure 4 shows the S 2p XPS spectra at the sulfide-treated n-Si surface. We found the S 2p peak located at 163.6 eV [33], indicating the presence of Si–S bonds. The presence of Si–S bonds has an effect on the Schottky barrier by reducing the interface state density, indicating that a good passivation is formed at the interface as a result of the reduction of the interfacial defect density [34]. Zhang et al. [35] suggested that the Si surface termination state plays key role on the electrical output of the Si-based devices. As compared to a graphene/as-cleaned n-Si Schottky diode, the number of charge traps in Si near the graphene/n-Si interface is significantly decreased for graphene/sulfide-treated n-Si Schottky diodes. Consequently, Si surface passivation reduced the number of charge traps, causing η_o (T_o) to decrease. In this report, we focused on the effects of the dangling bonds at the Si surface and suggested that it can be changed by the Si–S

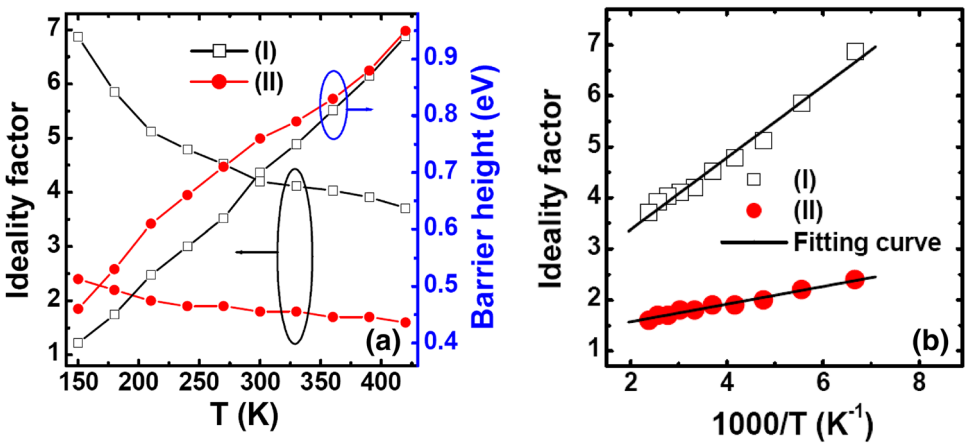

Fig. 3 **a** η ($q\phi_B$) as a function of temperature and **b** η as a function of 1,000/T [(I) graphene/as-cleaned n-Si and (II) graphene/sulfide-treated n-Si Schottky diodes]

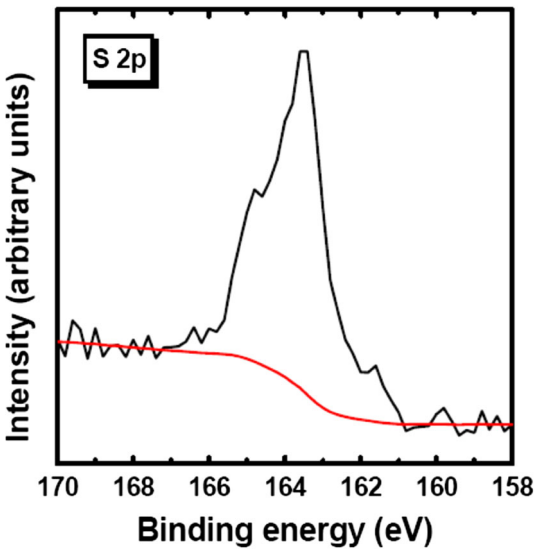

Fig. 4 S 2p XPS spectra at the sulfide-treated n-Si surface

bonding. We believe that the inhomogeneous barrier has a strong relation to the reduced number of charge traps on the n-Si sample; and, such result can be attributed to the Si–S bonding. Trap states in the Si near the graphene/Si interfaces were considered to affect interfacial barriers with contacts and consequently electrical leakage. We consider to the energy barrier lowering caused by trapped electrons jumping between the continuous potential well. The current will flow preferentially through the lower barriers in the potential distribution (that is, electrons hopping from one trap state to another trap state).

Figure 5 shows the conventional Richardson plot of $\ln(I_s/T^2)$ versus $10^3/T$ and the modified Richardson plot of $\ln(I_s/T^2)$ versus $10^3/(\eta T)$. As shown in Fig. 5, $\ln(I_s/T^2)$ versus $10^3/(\eta T)$ is more linear than $\ln(I_s/T^2)$ versus $10^3/T$ plot for the graphene/n-Si Schottky diode in temperature range measured. Bowing of the experimental $\ln(I_s/T^2)$ versus $10^3/T$ curve may be caused by the temperature dependence of $q\phi_B$ due to the existence of the Si surface inhomogeneities. We calculated the modified Richardson plots of $\ln(I_s/T^2)$ versus $10^3/(\eta T)$. The derived values of A^* are 1.2×10^{-5} A cm^{-2} K^{-2} for graphene/as-cleaned n-Si Schottky diodes and 4.3×10^{-5} A cm^{-2} K^{-2} for graphene/sulfide-treated n-Si Schottky diodes, which are not consistent with the theoretical value of 114 A cm^{-2} K^{-2}. The deviation may be due to the spatially inhomogeneous barriers and potential fluctuations at the interface that consist of low and high barrier areas, that is, the current through the diode will flow preferentially through the lower barriers in the potential distribution. The spatial barrier inhomogeneities in Schottky diodes are described by Gaussian distribution function [31, 36, 37]. The conventional Richardson plot is modified by Gaussian distribution function as follows [31, 37]:

$$\ln\left(\frac{I_s}{T^2}\right) - \frac{1}{2}\left(\frac{q\alpha_o}{kT}\right)^2 = \ln(SA^*) - \frac{q\phi_{B0}}{kT} \quad (2)$$

The standard deviation (α_o) is a measure of the barrier homogeneity. A modified $\ln(I_s/T^2) - q^2\alpha_o^2/2k^2T^2$ versus $1/T$ plot (Fig. 6) according to Eq (2) should give a straight line with the slope directly yielding the mean barrier height ($q\phi_{B0}$) and the intercept ($\ln SA^*$) at the ordinate determining A^*. The derived values of A^* are 92 A cm^{-2} K^{-2} for graphene/as-cleaned n-Si Schottky diodes and 106 A cm^{-2} K^{-2} for graphene/sulfide-treated n-Si Schottky diodes, which are close to the theoretical value of 114 A cm^{-2} K^{-2}. The values of $q\phi_{B0}$ (1.41 eV) and α_o (0.146 V) were obtained for graphene/as-cleaned n-Si Schottky diodes. The values of $q\phi_{B0}$ (1.41 eV) and α_o (0.136 V) were obtained for graphene/sulfide-treated n-Si Schottky diodes. α_o decreases while $q\phi_{B0}$ does not change substantially. The lower value of α_o corresponds to more homogenous barrier height. The improved barrier inhomogeneity by sulfide treatment may lead to a dramatic reduction in η. In addition, the derived value of $q\phi_{B0}$ by using the barrier inhomogeneity model is much larger than

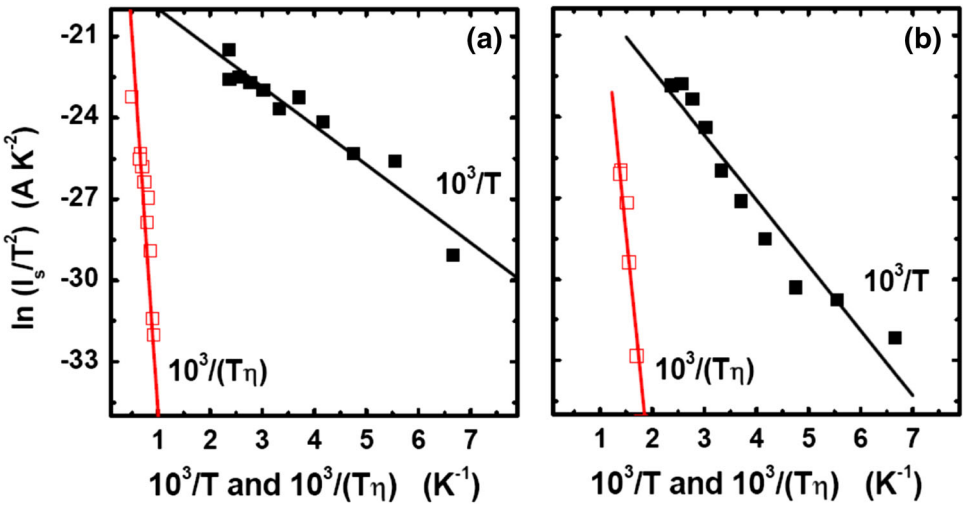

Fig. 5 Richardson plots of $\ln(I_s/T^2)$ versus $10^3(\eta T)^{-1}$ and $\ln(I_s/T^2)$ versus $10^3/T$ (**a** graphene/as-cleaned n-Si and **b** graphene/sulfide-treated n-Si Schottky diodes)

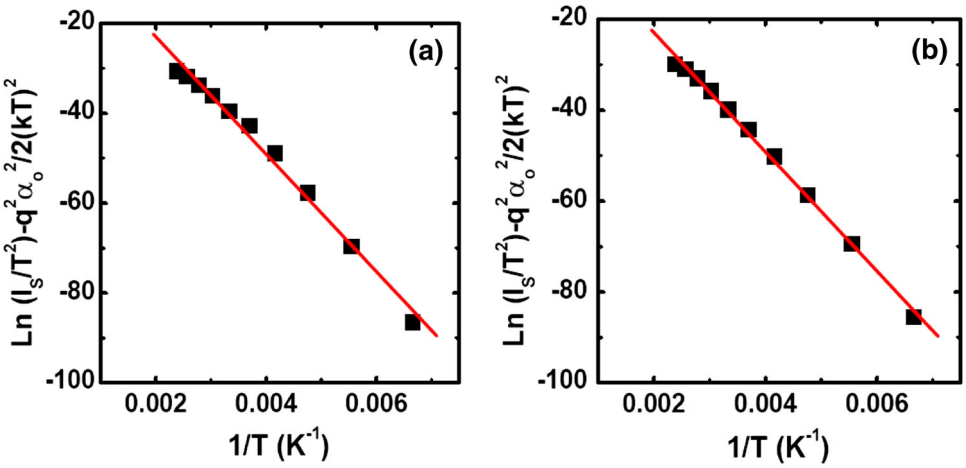

Fig. 6 Modified Richardson $\ln(I_s/T^2) - q^2\alpha_o^2/2k^2T^2$ versus $1/T$ plots for **a** graphene/as-cleaned n-Si and **b** graphene/sulfide-treated n-Si Schottky diodes according to Gaussian distribution of the barrier heights

the $q\phi_B$ values. This is due to the fact that $q\phi_B$ mainly reflects the lowest barrier height of local shallow patches, while $q\phi_{B0}$ reflects the average value of the fluctuating barriers.

In order to study the flowed current through the lower barriers (that is, the leakage current), the reverse-bias I–V characteristics are measured and compared at various temperatures. In the reverse-bias region, the leakage current is dominant. A probable reason for the large leakage current is the existence of the high interfacial defect density. Note, sulfide treatment is effective in passivating the n-Si surface and reducing the defect density at the graphene/n-Si interfaces, lowering the leakage current density. We suggest that the passivation of Si dangling bonds by S may lead to a reduction in the number of charge traps [34], improving the device performance. To determine whether the hopping conduction dominates the reverse-bias conduction behavior, analysis was conducted according to the log (I)–V relationship [38]. Figure 7 shows the reverse-bias current of the graphene/as-cleaned n-Si (graphene/sulfide-treated n-Si) device measured within a temperature range from 150 to 420 K. The leakage current is affected by sulfide treatment. The log (I)–V curves are almost linear and the conduction current increases as the temperature increases, which indicates that the reverse-bias currents exhibit hopping conduction behavior. The hopping conduction can be expressed as [38–40]

$$I = Sqa_m n_e v_f \left[\exp\left(\frac{qa_m V}{2dkT} - \frac{q\phi_t}{kT}\right)\right], \quad (2)$$

where a_m is the mean hopping distance, n_e is the density of space charge, v_f is the intrinsic vibration frequency, d is the film thickness and $q\phi_t$ is the barrier height for hopping. The inset of Fig. 7 shows the plot of $\ln(I)$ versus $(kT)^{-1}$ for $V = -2$, -3 and -4 V, respectively. The slope (S_L) is derived from Arrhenius plots (the inset of Fig. 7). Two curves are drawn, using a vertical axis of S_L and a lateral axis of V. The $q\phi_t$ derived from the S_L–V curve is about 154 (197) meV for graphene/n-Si (graphene/sulfide-treated n-Si) devices. Clearly, $q\phi_t$ is affected by sulfide

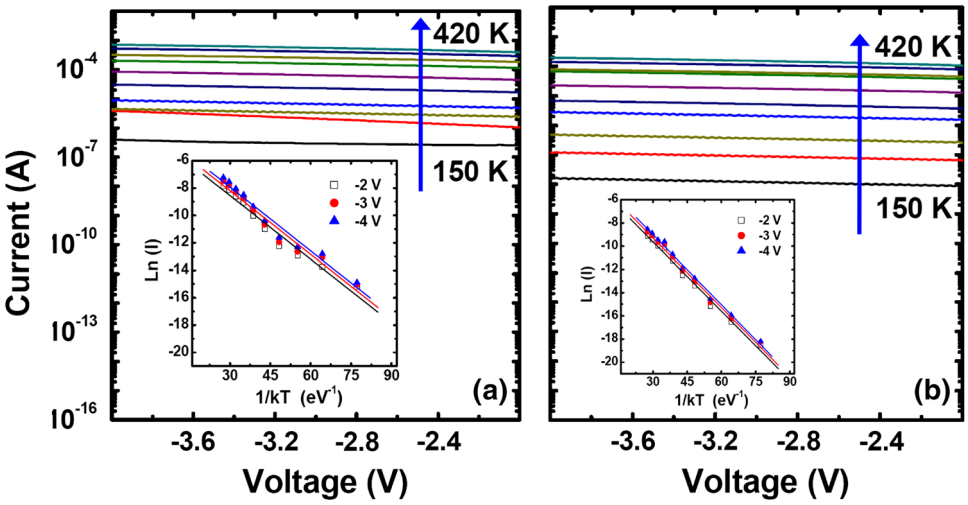

Fig. 7 The reverse-bias log(I)–V curves as a function of temperature (**a** graphene/as-cleaned n-Si and **b** graphene/sulfide-treated n-Si Schottky diodes). *Insets* plots of ln(I) versus $(kT)^{-1}$ for $V = -2$, -3 and -4 V

treatment. This is because of the presence of Si–S bonds that serve to improve the Schottky barrier inhomogeneity. Compared to the fitting data for the temperature-dependent reverse-bias I–V characteristics of graphene/as-cleaned n-Si devices, the fitting data for the temperature-dependent reverse-bias I–V characteristics of graphene/sulfide-treated n-Si devices show that a higher $q\phi_t$ result in a lower leakage current.

4 Conclusions

The effect of sulfide treatment on the temperature-dependent I–V characteristics of graphene/n-Si Schottky diodes is investigated. The value of A^* (106 A cm^{-2} K^{-2}) for graphene/sulfide-treated n-Si Schottky diodes was obtained by means of the modified Richardson plot considering Gaussian distribution of the barrier heights and this value is close to the theoretical value of electrons in n-Si. The enhanced device performance is considered to mainly come from the improved Schottky barrier inhomogeneity. The presence of Si–S bonds that serve to reduce the number of charge traps has a noticeable effect on Schottky barrier inhomogeneity. The improved device performance is also explained by a transition from hopping-dominated transport. The fitting data of the temperature-dependent I–V curves in the reverse-bias region demonstrate that the caused energy barrier lowering by trapped electrons hopping from one trap state to another trap state may lead to the formation of the inhomogeneous Schottky barrier heights.

Acknowledgments The authors acknowledge the support of the Ministry of Science and Technology of Taiwan (Contract No. 103-2112-M-018-003-MY3) in the form of grants.

References

1. S.D. Sarma, S. Adam, E.H. Hwang, E. Rossi, Rev. Mod. Phys. **83**, 407 (2011)
2. A.H. Castro Neto, F. Guinea, N.M.R. Peres, K.S. Novoselov, A.K. Geim, Rev. Mod. Phys. **81**, 109 (2009)
3. S. Tongay, T. Schumann, X. Miao, B.R. Appleton, A.F. Hebard, Carbon **49**, 2033 (2011)
4. S. Tongay, M. Lemaiyre, X. Miao, B. Gila, B.R. Appleton, A.F. Hebard, Phys. Rev. X **2**, 011002 (2012)
5. D. Dragoman, M. Dragoman, R. Plana, J. Appl. Phys. **108**, 084316 (2010)
6. C.C. Chen, M. Aykol, C.C. Chang, A.F.J. Levi, S.B. Cronin, Nano Lett. **11**, 1863 (2011)
7. M. Mohammed, Z. Li, J. Cui, T. Chen, Nanoscale Res. Lett. **7**, 302 (2012)
8. J.H. Lin, J.J. Zeng, Y.J. Lin, Thin Solid Films **550**, 582 (2014)
9. C. Yim, N. McEvoy, G.S. Duesberg. Appl. Phys. Lett. **103**, 193106 (2013)
10. X. Wang, K.Q. Peng, X.J. Pan, X. Chen, Y. Yang, L. Li, X.M. Meng, W.J. Zhang, S.T. Lee, Angew. Chem. Int. Ed. **50**, 9861 (2011)
11. D. Panda, T.Y. Tseng, Thin Solid Films **531**, 1 (2013)
12. W.M. Cho, Y.J. Lin, H.C. Chang, Y.H. Chen, Microelectron. Eng. **108**, 24 (2013)
13. S.Y. Myong, L.S. Jeon, S.W. Kwon, Thin Solid Films **550**, 705 (2014)
14. T. Tayagaki, Y. Hoshi, K. Ooi, T. Kiguchi, N. Usami, Thin Solid Films **557**, 368 (2014)
15. C.H. Ruan, Y.J. Lin, J. Appl. Phys. **114**, 143710 (2013)
16. S.C. Chen, T.C. Chang, Y.C. Wu, J.Y. Chin, Y.E. Syu, S.M. Sze, C.Y. Chang, H.H. Wu, Y.C. Chen, Thin Solid Films **518**, 3999 (2010)
17. C.C. Huang, Y.J. Lin, C.J. Liu, Y.W. Yang, Microelectron. Eng. **110**, 21 (2013)
18. Y.M. Chin, Y.J. Lin, Mater. Chem. Phys. **145**, 232 (2014)
19. X. Li, H. Zhu, K. Wang, A. Cao, J. Wei, C. Li, Y. Jia, Z. Li, X. Li, D. Wu, Adv. Mater. **22**, 2743 (2010)
20. Y.J. Lin, B.C. Huang, Y.C. Lien, C.T. Lee, C.L. Tsai, H.C. Chang, J. Phys. D Appl. Phys. **42**, 165104 (2009)
21. Y.J. Lin, J.J. Zeng, Appl. Phys. Lett. **102**, 183120 (2013)
22. A. Mooradian, Phys. Rev. Lett. **22**, 185 (1969)

23. S.D. Costa, A. Righi, C. Fantini, Y. Hao, C. Magnuson, L. Colombo, R.S. Ruoff, M.A. Pimenta, Solid State Commun. **152**, 1317 (2012)
24. Q. Yu, J. Lian, S. Siriponglert, H. Li, Y.P. Chen, S.S. Pei, Appl. Phys. Lett. **93**, 113103 (2008)
25. S.J. Chae, F. Güneş, K.K. Kim, E.S. Kim, G.H. Han, S.M. Kim, H.J. Shin, S.M. Yoon, J.Y. Choi, M.H. Park, C.W. Yang, D. Pribat, Y.H. Lee, Adv. Mater. **21**, 2328 (2009)
26. J.J. Zeng, Y.J. Lin, Appl. Phys. Lett. **104**, 233103 (2014)
27. K.N. Kudin, B. Ozbas, H.C. Schniepp, R.K. Prud'homme, I.A. Aksay, R. Car. Nano Lett. **8**, 36 (2008)
28. G. Eda, G. Fanchini, M. Chhowalla, Nat. Nanotechnol. **3**, 270 (2008)
29. Z. Luo, N.J. Pinto, Y. Davila, A.T. Charlie, Johnson. Appl. Phys. Lett. **100**, 253108 (2012)
30. R.T. Tung, Phys. Rev. B **45**, 13509 (1992)
31. Ş. Karataş, Ş. Altındal, Mater. Sci. Eng., B **122**, 133 (2005)
32. S. Zhu, R.L. Van Meirhaeghe, C. Detavernier, F. Cardon, G.P. Ru, X.P. Qu, B.Z. Li, Solid State Electron. **44**, 663 (2000)
33. H. Peisert, T. Chasse, P. Streubel, A. Meisel, R. Szargan, J. Electron Spectrosc. Relat. Phenom. **68**, 321 (1994)
34. G. Song, M.Y. Ali, M. Tao, Solid-State Electron. **52**, 1778 (2008)
35. F. Zhang, D. Liu, Y. Zhang, H. Wei, T. Song, B. Sun, ACS Appl. Mater. Interf. **5**, 4678 (2013)
36. P.G. McCafferty, A. Sellai, P. Dawson, H. Elabd, Solid State Electron. **39**, 583 (1996)
37. I. Taşçıoğlu, U. Aydemir, Ş. Altındal, J. Appl. Phys. **108**, 064506 (2010)
38. K.C. Chang, T.M. Tsai, R. Zhang, T.C. Chang, K.H. Chen, J.H. Chen, T.F. Young, J.C. Lou, T.J. Chu, C.C. Shih, J.H. Pan, Y.T. Su, Y.E. Syu, C.W. Tung, M.C. Chen, J.J. Wu, Y. Hu, S.M. Sze, Appl. Phys. Lett. **103**, 083509 (2013)
39. T.H. Su, Y.J. Lin, Appl. Phys. Lett. **104**, 153504 (2014)
40. Y.J. Lin, Y.C. Lin, Appl. Phys. Lett. **105**, 023506 (2014)